A Spectral Lanczos Decomposition Method for Solving 3-D Low-Frequency Electromagnetic Diffusion by the Finite-Element Method

Mohammad R. Zunoubi, *Member, IEEE,* Jian-Ming Jin, *Senior Member, IEEE,*
Kalyan C. Donepudi, and Weng Cho Chew, *Fellow, IEEE*

***Abstract*— A very efficient three-dimensional (3-D) solver for the diffusion of the electromagnetic fields in an inhomogeneous medium is described. The proposed method employs either the node-based or the edge-based finite-element method (FEM) to discretize Maxwell's equations. The resultant matrix equation is solved by the spectral Lanczos decomposition method (SLDM), which is based on the Krylov subspace (Lanczos) approximation of the solution in frequency domain. By analyzing some practical geophysical problems, it is shown that the SLDM is extremely fast and, furthermore, the electromagnetic fields at many frequencies can be evaluated by performing the SLDM iteration only at the lowest frequency.**

***Index Terms*— Electromagnetic diffusion, fast solvers, finite-element methods.**

I. Introduction

THE dual laterlog operating over a wide range of frequencies has been used traditionally to investigate the resistivity profile of formations. These resistivities are used to estimate the amount of hydrocarbon in rocks [1]. In simple layered media, the tool response can be obtained by using spectral fast Fourier transform (FFT) techniques [2], [3]. However, when the geometry includes multiple beds, a borehole, and invaded beds, the problem can be solved only by semi-analytic or finite-element techniques [4], [5]. The finite-element method (FEM) has been used as the most popular technique to simulate well logging problems. It has been applied by Zhang [6] to model laterlog tools, by Anderson and Chang [7] to synthesize the induction tool responses, and by Li and Shen [8] to simulate spherically focused logs. A thorough study of the FEM application in well logging simulation is given by Lovell [1].

Although the FEM has been applied in well logging problems, all the techniques presented so far suggest obtaining solutions independently for every frequency over a wide spectrum of frequencies. This, however, proves to be extremely time consuming for multiple frequency simulations. Recently, Druskin and Knizhnerman [9] have introduced a new technique called the spectral Lanczos decomposition method (SLDM), which is capable of solving Maxwell's equations for many frequencies in a negligible amount of extra computing time. The method has been applied to solve for electromagnetic fields discretized by the finite-difference method (FDM). It was recently employed for solving axisymmetric low-frequency electromagnetic diffusion by the FEM [10].

When Maxwell's equations are discretized by either the finite-element or FDM, the resulting equation may be cast into a matrix equation

$$Ax + j\omega\mu Cx = b \tag{1}$$

where A and C are typically real-square matrices, x is the unknown vector, and b is the excitation vector. This matrix equation can be modified as

$$A'x + j\omega\mu Ix = b' \tag{2}$$

where I is the identity matrix. The SLDM solves (2) using approximations in a global Krylov subspace to the product of a matrix and a vector using the Lanczos method.

In this work, the FEM is employed to discretize Maxwell's equations in a low-frequency regime for three-dimensional (3-D) problems. The SLDM is then applied to the resulting matrix equation to solve for the electromagnetic fields for multiple frequencies. The problems treated here are assumed to involve dielectrics only and, hence, the magnetic field formulation is employed.

II. Finite-Element Formulation

When electromagnetic problems are analyzed by the FEM, Maxwell's equations can be discretized by either node-based elements or edge-based elements. In this section, both discretization methods are discussed.

A. Node-Based Elements

In a low-frequency regime where the effect of displacement currents can be neglected, Maxwell's equations are given by

$$\nabla \times \mathbf{H} = \overline{\overline{\sigma}} \cdot \mathbf{E} + \mathbf{J}, \qquad \nabla \times \mathbf{E} = -j\omega\mu\mathbf{H} \tag{3}$$

which can be solved for either the electric field intensity $\mathbf{E}$ or the magnetic field intensity $\mathbf{H}$. Here, $\overline{\overline{\sigma}}$ denotes a diagonal

Manuscript received August 12, 1997; revised July 17, 1998. This work was supported by a gift from Mobil Research Corporation, a grant from AFOSR via the MURI Program under Contract F49620-96-1-0025, the Office of Naval Research under Grants N00014-95-1-0848 and N00014-95-1-0872, and the National Science Foundation under Grants NSF ECS 94-57735 and ECS 93-02145.

The authors are with the Center for Computational Electromagnetics, Department of Electrical and Computer Engineering, University of Illinois at Urbana-Champaign, Urbana, IL 61801 USA.

Publisher Item Identifier S 0018-926X(99)03734-5.

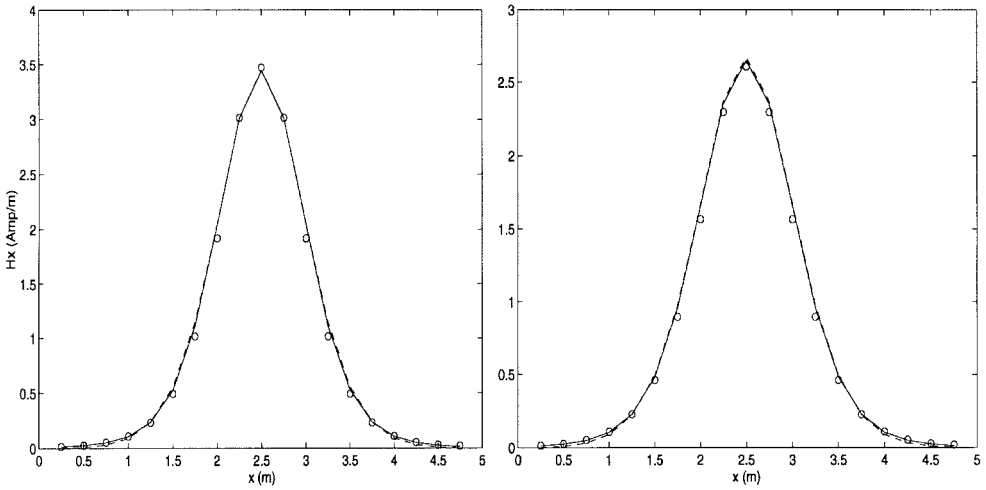

(a) (b)

Fig. 1. Magnitude of the x component of the magnetic field at $z = 1.5$ m. (a) $y = 2.25$ m. (b) $y = 2.0$ m (- - - analytical; ——— FEM with tetrahedral nodal elements; ∘ FDM).

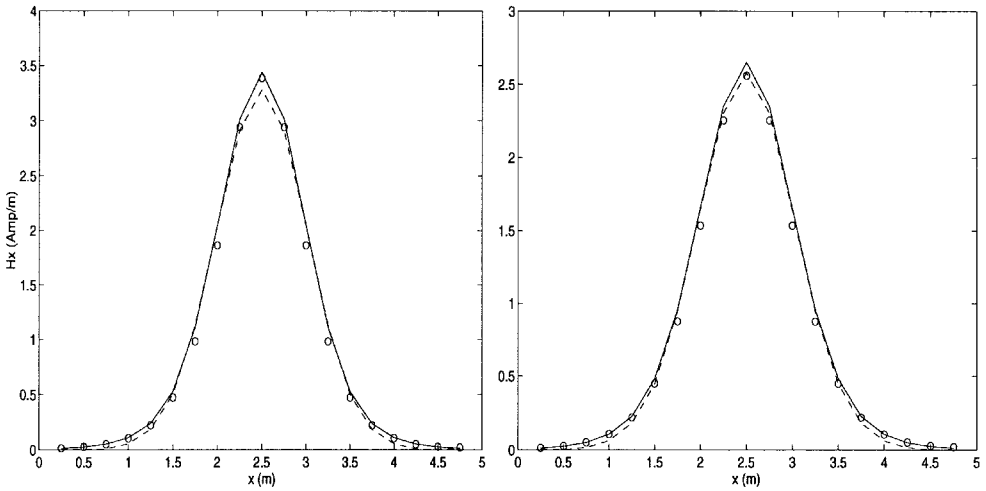

(a) (b)

Fig. 2. Magnitude of the x component of the magnetic field at $z = 1.5$ m. (a) $y = 2.25$ m. (b) $y = 2.0$ m (- - - analytical; ——— FEM with brick nodal elements; ∘ FEM with edge elements).

tensor which accounts for the anisotropy of the electrical conductivity. If (3) is solved for the $\mathbf{H}$-field, we obtain

$$\nabla \times \left(\overline{\overline{\sigma}}^{-1} \cdot \nabla \times \mathbf{H}\right) + j\omega\mu\mathbf{H} = \mathbf{M} \tag{4}$$

where $\mathbf{M} = \nabla \times (\overline{\overline{\sigma}}^{-1} \cdot \mathbf{J})$. For simplicity, we choose the outer boundaries sufficiently far from the source so that the field satisfies the boundary condition

$$\hat{n} \times \mathbf{H} = \mathbf{0}. \tag{5}$$

In accordance with the variational principle, the solution to (4) and (5) is obtained [11] by extremizing the functional

$$F(\mathbf{H}) = \tfrac{1}{2} \iiint_V \left\{\left(\overline{\overline{\sigma}}^{-1} \cdot \nabla \times \mathbf{H}\right) \cdot (\nabla \times \mathbf{H}) + s(\nabla \cdot \mathbf{H})^2 + j\omega\mu\mathbf{H} \cdot \mathbf{H}\right\} dV - \iiint_v \mathbf{M} \cdot \mathbf{H}\, dV \tag{6}$$

where s is a penalty factor and its associated term is called the penalty term, which is included to suppress spurious modes in the solution. To discretize (6), we subdivide the volume V into M small volume elements such as tetrahedral or rectangular elements. The magnetic field can then be expanded as

$$\begin{aligned}\mathbf{H}(x, y, z) &= \sum_{i=1}^{N} N_i(x, y, z)(\hat{x}H_{xi} + \hat{y}H_{yi} + \hat{z}H_{zi}) \\ &= \{N\}^T(\hat{x}\{H_x\} + \hat{y}\{H_y\} + \hat{z}\{H_z\})\end{aligned} \tag{7}$$

where N denotes the total number of nodes, and $N_i(x, y, z)$ denotes the expansion function associated with node i and H_{xi}, H_{yi}, and H_{zi} are the magnetic field components at node i. Next, substituting (7) into (6) and applying the Rayleigh–Ritz procedure, one obtains

$$\begin{bmatrix} K_{xx} & K_{xy} & K_{xz} \\ K_{yx} & K_{yy} & K_{yz} \\ K_{zx} & K_{zy} & K_{zz} \end{bmatrix} \begin{Bmatrix} H_x \\ H_y \\ H_z \end{Bmatrix} + j\omega\mu \begin{bmatrix} T_{xx} & 0 & 0 \\ 0 & T_{yy} & 0 \\ 0 & 0 & T_{zz} \end{bmatrix} \begin{Bmatrix} H_x \\ H_y \\ H_z \end{Bmatrix} = \begin{Bmatrix} b_x \\ b_y \\ b_z \end{Bmatrix} \tag{8}$$

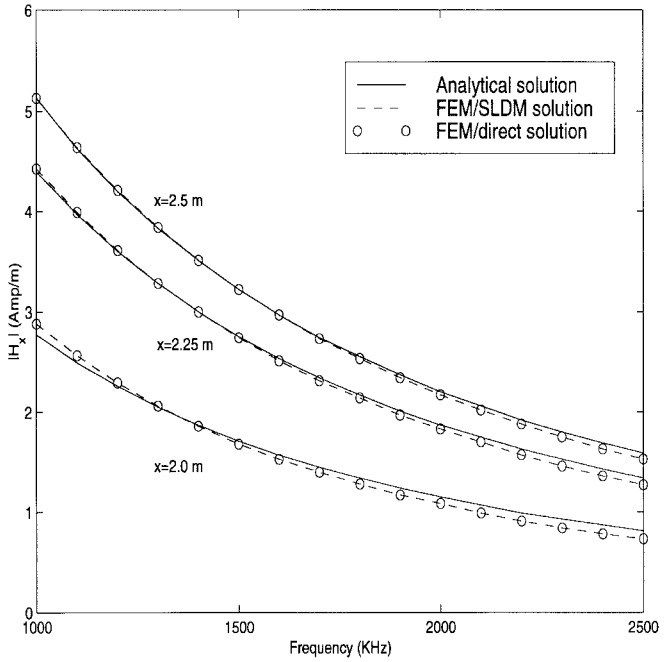

Fig. 3. Magnitude of the x component of magnetic field at $y = 1.75$ m and $z = 2.0$ m.

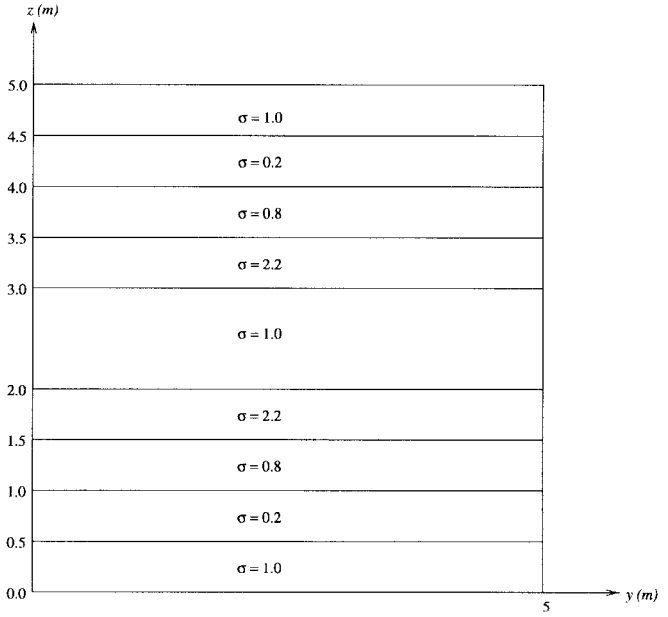

Fig. 4. Cross-sectional view of the problem geometry for the magnetic field computation of an inhomogeneous medium.

where

$$[K_{xx}] = \iiint_V \left(s \frac{\partial\{N\}}{\partial x} \frac{\partial\{N\}^T}{\partial x} + \frac{1}{\sigma_z} \frac{\partial\{N\}}{\partial y} \frac{\partial\{N\}^T}{\partial y} + \frac{1}{\sigma_y} \frac{\partial\{N\}}{\partial z} \frac{\partial\{N\}^T}{\partial z} \right) dV$$

$$[K_{yy}] = \iiint_V \left(\frac{1}{\sigma_z} \frac{\partial\{N\}}{\partial x} \frac{\partial\{N\}^T}{\partial x} + s \frac{\partial\{N\}}{\partial y} \frac{\partial\{N\}^T}{\partial y} + \frac{1}{\sigma_x} \frac{\partial\{N\}}{\partial z} \frac{\partial\{N\}^T}{\partial z} \right) dV$$

$$[K_{zz}] = \iiint_V \left(\frac{1}{\sigma_y} \frac{\partial\{N\}}{\partial x} \frac{\partial\{N\}^T}{\partial x} + \frac{1}{\sigma_x} \frac{\partial\{N\}}{\partial y} \frac{\partial\{N\}^T}{\partial y} + s \frac{\partial\{N\}}{\partial z} \frac{\partial\{N\}^T}{\partial z} \right) dV$$

$$[K_{pq}] = \iiint_V \left(s \frac{\partial\{N\}}{\partial p} \frac{\partial\{N\}^T}{\partial q} - \frac{1}{\sigma_r} \frac{\partial\{N\}}{\partial q} \frac{\partial\{N\}^T}{\partial p} \right) dV \quad p, q, r = x, y, z;\ r \neq p \neq q$$

$$[T_{pp}] = \iiint_V \{N\}\{N\}^T dV \qquad p = x, y, z$$

$$\{b_p\} = \iiint_V \{N\} M_p dV \qquad p = x, y, z. \tag{9}$$

For simplicity, (8) can be written in a compact form as

$$([C] + j\omega\mu[T])\{H\} = \{b\} \tag{10}$$

where C and T are called the *stiffness* and *mass* matrices, respectively. This matrix equation can be solved by the SLDM which is discussed in detail in Section III.

B. Edge-Based Elements

As discussed above, the existence of spurious modes can be suppressed by introducing a penalty factor in the FEM formulations when node-based elements are used. Another approach for achieving the same objective is to use vector basis functions or vector elements in place of nodal elements [11]. The solution of (4) and (5) is obtained by seeking the stationary point of the functional given by

$$F(\mathbf{H}) = \tfrac{1}{2} \iiint_V \left[(\bar{\bar{\sigma}}^{-1} \cdot \nabla \times \mathbf{H}) \cdot (\nabla \times \mathbf{H}) + j\omega\mu \mathbf{H} \cdot \mathbf{H} \right] dV - \iiint_v \mathbf{M} \cdot \mathbf{H}\, dV \tag{11}$$

where V denotes the volume of interest. This functional can be discretized by first subdividing the volume V into small elements and expanding the magnetic field as

$$\mathbf{H}(x, y, z) = \sum_{i=1}^{N} \mathbf{N}_i(x, y, z) H_i \tag{12}$$

where $\mathbf{N}_i$ denotes the expansion function associated with edges and H_i denotes the associated tangential magnetic field. Substituting (12) into (11) and applying the Rayleigh–Ritz procedure, we obtain the matrix equation

$$([C] + j\omega\mu[T])\{H\} = \{b\} \tag{13}$$

where $\{H\} = [H_1, H_2, \cdots, H_N]^T$ and

$$C_{i,j} = \iiint_V (\bar{\bar{\sigma}}^{-1} \cdot \nabla \times \mathbf{N}_i) \cdot (\nabla \times \mathbf{N}_j)\, dV$$

$$T_{i,j} = \iiint_V \mathbf{N}_i \cdot \mathbf{N}_j\, dV$$

$$b_i = \iiint_V \mathbf{N}_i \cdot \mathbf{M}\, dV. \tag{14}$$

Note that (13) has a similar form to (10), which can be solved by the SLDM.

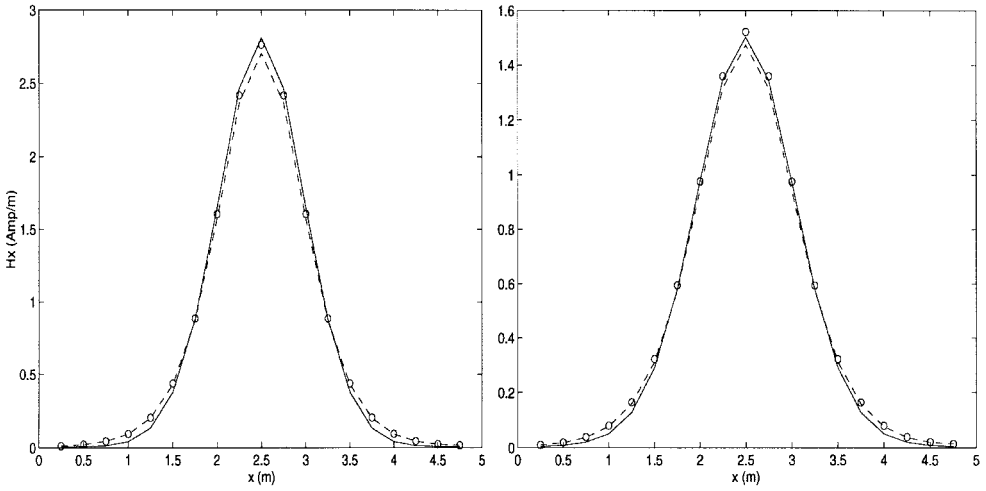

(a) (b)

Fig. 5. Magnitude of the x component of the magnetic field at $z = 1.75$ m. (a) $y = 1.75$ m. (b) $y = 1.5$ m (- - - FEM with nodal elements; ——— FEM with edge elements; ∘ FDM).

TABLE I
CPU TIME AND THE NUMBER OF ITERATIONS FOR THE SLDM WITH 21 660 UNKNOWNS FOR THE M_x EXCITATION

Method	CPU time (s) 1,000 KHz		CPU time (s) 1,000-2,500 KHz		Iterations
	assemble	Lanczos	assemble	Lanczos	
FDM	1.1	12.9	1.1	15.3	56
FEM-vector	3.6	16.8	3.6	18.8	45
FEM-nodal	8.3	20.0	8.3	21.3	29

III. SPECTRAL LANCZOS DECOMPOSITION METHOD

In order to solve either (10) or (13) for the magnetic field by the SLDM [9], this equation must be first cast to a form

$$(A + j\omega\mu I)x = u \tag{15}$$

with I being the identity matrix. Therefore, we convert the matrix T of (10) or (13) to a diagonal matrix by the row-sum lumping procedure to obtain

$$(C + j\omega\mu D)\Phi = b \tag{16}$$

where $\Phi = \{H\}$. For the sake of convenience, the brackets are omitted for the notation of matrices and vectors in this section. Equation (16) can be further written as

$$\left(D^{-1/2} C D^{-1/2} + j\omega\mu I\right)\Phi' = D^{-1/2} b \tag{17}$$

or

$$(A' + j\omega\mu I)\Phi' = b' \tag{18}$$

with $\Phi' = D^{1/2}\Phi$. The solution of (18) can be expressed as

$$\Phi' = (A' + j\omega\mu I)^{-1} b'. \tag{19}$$

We approximate the unknown vector Φ' in the above equation in the SLDM by replacing the matrix A' with its $M(<N)$ eigenvalues and corresponding eigenvectors which are obtained from a symmetric tridiagonal matrix H referred to as the Ritz approximation of A'. H is generated from A' via an orthogonal transformation, or more specifically, the Lanczos process and is related to A' as

$$Q^T A' Q = H \tag{20}$$

where $Q = [q_1, q_2, \cdots, q_M]$ is an orthogonal matrix. We generate the bases $q_1, q_2, \cdots, q_M$ by the Gram–Schmidt orthogonalization process of vectors b', $A'b'$, $\cdots$, $A'^{M-1}b'$ in the Krylov subspace

$$\kappa(A', q_1, M) = \text{span}\{q_1, A'q_1, \cdots, A'^{M-1}q_1\}. \tag{21}$$

If we define the elements of the Ritz matrix H as

$$\begin{aligned} H_{i,i} &= \alpha_i, \qquad i = 1, 2, \cdots, M \\ H_{i,i-1} &= H_{i-1,i} = \beta_i, \qquad i = 1, 2, \cdots, M-1 \end{aligned} \tag{22}$$

then (20) can be written as

$$A'q_i = \beta_{i-1}q_{i-1} + \alpha_i q_i + \beta_i q_{i+1}, \qquad i = 1, \cdots, M-1 \tag{23}$$

where $\beta_0 q_0 = 0$. The orthonormality of q_i implies that

$$\alpha_i = q_i^T A' q_i. \tag{24}$$

If we define the vector r_i as

$$r_i = (A' - \alpha_i I)q_i - \beta_{i-1}q_{i-1} \neq 0 \tag{25}$$

then q_{i+1} can be expressed as

$$q_{i+1} = \frac{r_i}{\beta_i} \tag{26}$$

where $\beta_i = \|r_i\|_2$. The Lanczos process is defined by (22)–(26) and it is used to construct the tridiagonal matrix H and the orthogonal matrix Q. We further define Λ and V to be the eigenvalues and their corresponding eigenvectors of matrix H, respectively, and

$$H = V\Lambda V^T, \qquad \Lambda = \text{diag}[\lambda_1, \lambda_2, \cdots, \lambda_M]. \tag{27}$$

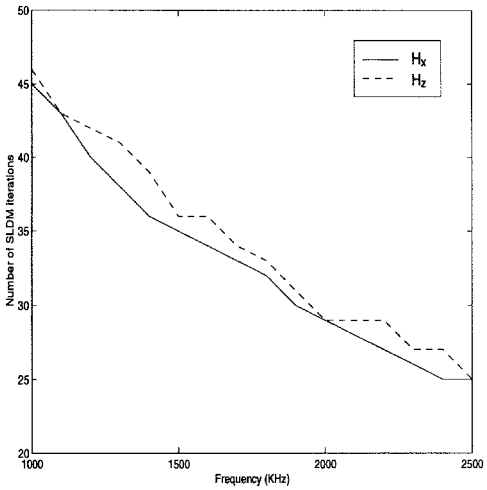

Fig. 6. Number of SLDM iterations for calculating H_x and H_z at each frequency.

TABLE II
CPU TIME REQUIRED FOR ASSEMBLING THE MATRICES

Unknowns	FDM	FEM-vector	FEM-nodal
	CPU time (s)	CPU time (s)	CPU time (s)
21,660	1.1	3.6	8.3
38,088	2.1	6.4	16.1
75,690	4.7	13.4	32.9
111,078	6.6	20.6	49.8
182,520	10.9	39.5	90.9

A vector q_1 is chosen as

$$q_1 = Qe_1 = \frac{b'}{||b'||} \tag{28}$$

where $e_1 = (1, 0, 0, \cdots, 0)^T$ is the first unit M vector. The unknown Φ' in (19) is then approximated by

$$\Phi' \approx ||b'||QV(\Lambda + j\omega\mu I)^{-1}V^T e_1 \tag{29}$$

which is a valid approximation of the unknown vector Φ' since the spectrum of H is contained in the spectral segment of matrix A'.

It is apparent that the main arithmetic work in the SLDM concerns the construction of matrices Q and H. However, the dimension of the Krylov subspace, M, necessary to reach convergence is typically much smaller than the dimension of matrix A', N [9]. To compute the eigenvalues and eigenvectors of H, we implement the PWK [12] and inverse-iteration algorithms, respectively. With the above algorithms, only $O(m^2)$ operation are required to generate the eigenpairs. It must be also noted that the matrices Q and H are not recomputed for multiple frequency analysis. As such, only the matrix functional $f(H)$ of (29) is computed for at each single frequency. This is the most attractive feature of the SLDM. Therefore, the SLDM allows for obtaining solution for multiple frequency simulations by generating matrices Q and H only once while recomputing the matrix functional $(\Lambda + j\omega\mu I)^{-1}$ at each frequency. We verify this fact in Section IV.

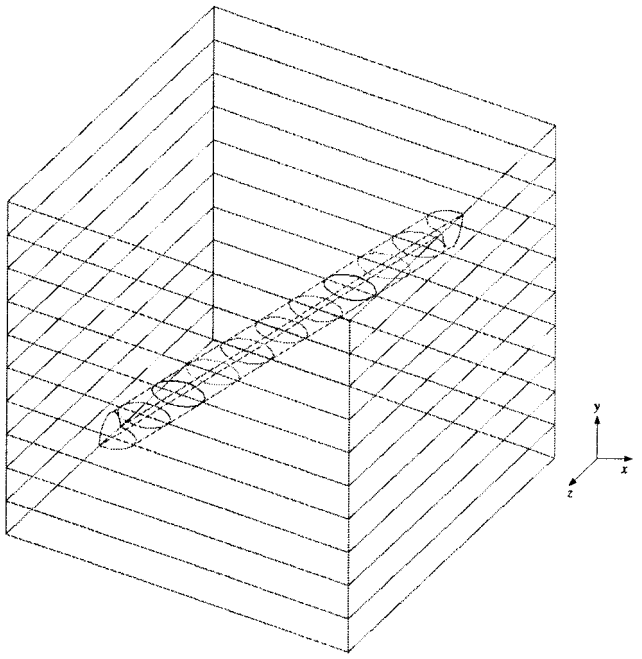

(a)

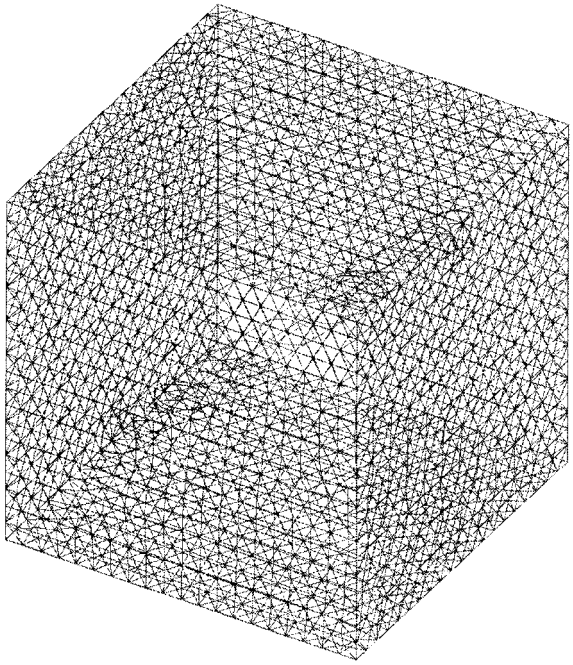

(b)

Fig. 7. (a) The problem geometry of a borehole penetrating layered beds at an angle of 45°. The electrical conductivity of each layer from top to bottom is 0.35, 0.5, 0.25, 0.4, 0.6, 0.6, 0.2, 0.05, 0.1, and 0.15 and that of the borehole is 1.0. (b) The finite-element mesh.

IV. RESULTS

To verify the formulation presented in this work, some practical geophysical problems are analyzed. The geometry considered first is a homogeneous cubic region of length 5 m and a unit electrical conductivity. For simplicity, only an x component of the magnetic current density is used to excite the region. The region is subdivided into 20 segments in each direction resulting in a total of 20 577 unknowns.

TABLE III
CPU TIME FOR THE SLDM AND THE NUMBER OF ITERATIONS

Unknowns	FDM		FEM-vector		FEM-nodal	
	CPU time (s)	iterations	CPU time (s)	iterations	CPU time (s)	iterations
21,660	12.9	56	16.8	45	20.0	29
38,088	50.2	93	27.5	40	33.6	26
75,690	39.1	44	48.8	34	63.2	23
111,078	57.2	42	65.5	32	90.0	22
182,520	82.5	37	104.1	28	139.0	21

The magnitude of the x component of the magnetic field is computed at a frequency of 1000 KHz and the results are compared with the corresponding results obtained from the FDM and the analytical solution. Comparisons of the results are shown in Figs. 1 and 2. Since the magnetic current source is positioned at the center of the region, results are given at a few planes away from the source location. As can be seen from these figures, both the analytical and the FDM results are in good agreement with the corresponding results obtained from the FEM technique. It is also worthwhile to note that the penalty factor s is set at 0.5 for this study, which proves to be an optimum value. To investigate the accuracy of our multiple frequency analysis of the field by the SLDM, the same Q and H matrices generated at 1000 KHz are used to obtain results in a frequency range of 1000–2500 KHz with an increment of 100 KHz. Fig. 3 shows a comparison with the corresponding analytical and finite-element direct solutions. The tetrahedral elements are used here for discretization purposes. As can be seen from this figure, a very good agreement is obtained. Note that the discrepancy between the results becomes larger as the frequency increases. This is due to the fact that the analytical solution is a full-wave solution.

Next, an inhomogeneous medium with the cross-section shown in Fig. 4 is considered. The x component of the magnetic field is calculated by the FEM using both the node-based and the edge-based elements at $f = 1000$ KHz and the results are compared with the corresponding FDM results. As can be seen in Fig. 5, a very good agreement is obtained. Additionally, the z component of the magnetic field is computed due to a z-directed magnetic current source and the same accuracy as shown in Fig. 5 for the M_x excitation is achieved.

In order to illustrate the effectiveness of the SLDM, a multiple frequency analysis of the magnetic field is performed first, when the geometry of Fig. 4 is excited by both M_x and M_z. A frequency range of 1000–2500 KHz is considered. The results are obtained by the SLDM for $f = 1000$ KHz while the same Q and H matrices are used to evaluate the field at the remaining frequencies (see Fig. 6). Results are given in Table I for the M_x excitation and those for the M_z excitation are similar. As can be seen from this table, only about two seconds extra are needed to compute the magnetic field at 15 additional frequencies using either the FEM or the FDM. To further justify the multiple-frequency results, the SLDM is employed to compute the field at each single frequency in the above frequency range and the number of SLDM iterations is plotted in Fig. 7. Note that only the FEM with the edge elements is used for this illustration. It is seen that

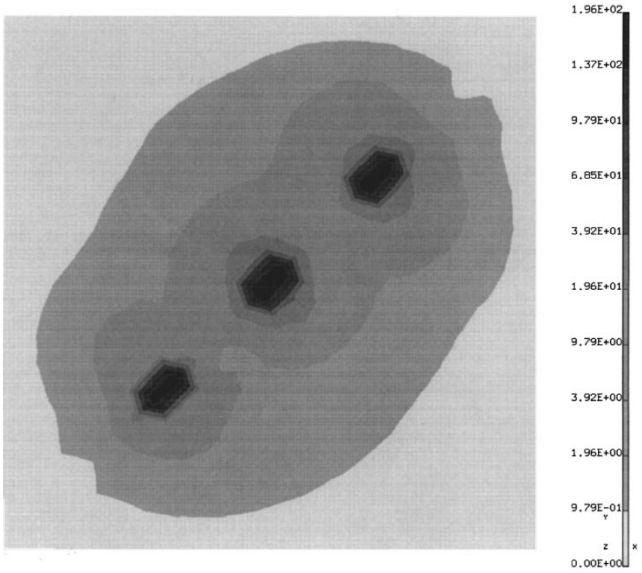

Fig. 8. Magnitude of the total magnetic field on xy plane and $z = 2.5$ m.

as the frequency increases, the number of iterations decreases accordingly. Therefore, the same Q and H matrices formed at 1000 KHz can be used to evaluate the field at higher frequencies. Furthermore, the total CPU time for obtaining results at each single frequency is estimated to be 253.87 s compared to only 18.8 s required for multiple-frequency analysis for M_x excitation while the CPU times for the M_z excitation are 262.34 and 22.5 s, respectively. The saving in the CPU time would be more significant if more frequency points are considered.

Next, the geometrical size of Fig. 4 is extended from 5 m $\times$ 5 m $\times$ 5 m to 10 m $\times$ 10 m $\times$ 10 m with the number of unknowns growing from 20 577 to 182 520. Table II presents the CPU time required for assembling the matrices of either (10) or (13). The CPU time required to solve the system of equations and the number of SLDM iterations are shown in Table III. It is seen that the CPU time reaches only 82.5, 104.1, and 139.0 s using the FDM, the FEM with edge elements, and the FEM with nodal elements, respectively. It is to be noted that the number of nonzero entries of matrix A is different in the FEM with node-based and edge-based elements, and the FDM. Therefore, although the number of SLDM iterations may be the same for all three methods, the CPU time will be different due to the difference in performing the matrix-vector multiplication.

Finally, the effectiveness of the method is tested by considering a practical problem of a cylindrical borehole penetrating layered beds with various electrical conductivities at an angle

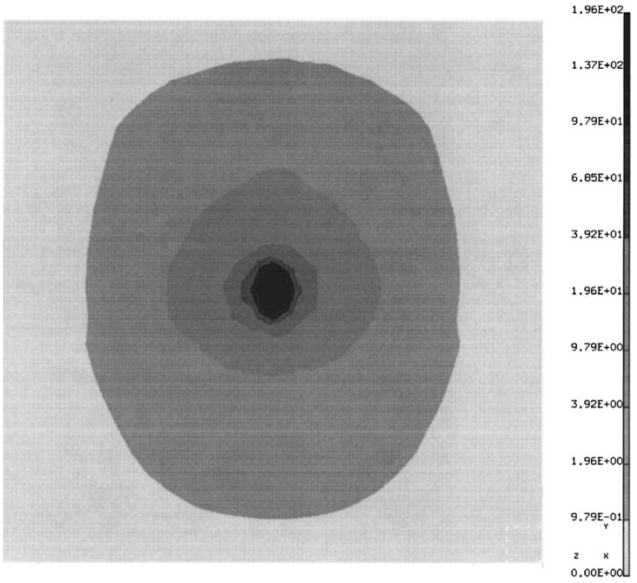

Fig. 9. Magnitude of the total magnetic field on yz plane and $x = 2.5$ m.

of 45°. The problem geometry and the finite-element mesh generated using SDRC-IDEAS are seen in Fig. 8. The geometrical size of the problem is 5 m × 5 m × 5 m. The mesh contains 55 798 tetrahedra, 10 693 nodes, and 24 807 unknowns. To simulate the current sources, three electric dipoles of a finite length and separated by a distance of 0.5 m are positioned inside the borehole. The magnetic field intensity is computed by the SLDM at $f = 1000$ KHz and the magnitude of the total magnetic field is plotted on xy plane at $z = 2.5$ m and on yz plane at $x = 2.5$ m. Results are shown in Fig. 9, clearly indicating the inhomogeneity of the solution domain. The total CPU time was approximately 210.0 s. The accuracy criterion (the relative difference between two consecutive iterations) in above computations is 10^{-6} and all the computations are performed on a DEC Alpha Workstation computer with an average throughput of 44 MFlops.

V. Conclusion

The spectral Lanczos decomposition method is applied to the solution of the general 3-D Maxwell's equations in a low-frequency regime when the FEM with both the node-based elements and the edge-based elements is employed to discretize Maxwell's equations. The formulation presented here is validated by comparing the results with the corresponding analytical results obtained for homogeneous configurations and the FDM results for more complicated geometries. The problems considered are of a practical geophysical nature. It is shown that the SLDM is not only computationally fast, but also capable of obtaining solutions at many frequencies by performing the SLDM iterations only for the lowest frequency of interest.

References

[1] J. R. Lovell, *Finite-Element Methods in Resistivity Logging.* Ridgefield, CT: Schlumberger Technol., 1993.

[2] B. Anderson, "Induction sonde response in stratified media," *Log Analyst*, vol. 24, no. 1, pp. 25–31, 1983.

[3] W. C. Chew, *Waves and Fields in Inhomogeneous Media.* New York: Van Nostrand Reinhold, 1990.

[4] W. C. Chew, S. Barone, B. Anderson, and C. Hennessy, "Diffraction of axisymmetric waves in a borehole by bed boundary discontinuities," *Geophys.*, vol. 49, no. 10, pp. 1586–1595, 1984.

[5] W. C. Chew, Z. Nie, Q.-H. Liu, and B. Anderson, "An efficient solution for the response of electrical well logging tools in a complex environment, " *IEEE Trans. Geosci. Remote Sensing*, vol. 29, no. 2, pp. 308–313, Mar. 1991.

[6] G. J. Zhang, *Electrical Well Logging.* Beijing, China: Petroleum Indust, 1986.

[7] B. Anderson and S. K. Chang, "Synthetic induction logs by the finite-element," *Log Analyst*, vol. 23, pp. 17–26, 1982.

[8] J. Li and L. C. Shen, "Numerical simulation of spherically focused logs," *Log Analyst*, vol. 33, pp. 495–499, 1992.

[9] V. Druskin and L. Knizhnerman, "Spectral approach to solving three-dimensional Maxwell's diffusion equations in the time and frequency domains," *Radio Sci.*, vol. 29, no. 4, pp. 937–953, Aug. 1994.

[10] M. Zunoubi, J. M. Jin, and W. C. Chew, "A spectral Lanczos decomposition method for solving axisymmetric low-frequency electromagnetic diffusion by the finite-element method," *J. Electromagn. Waves Applicat.*, to be published.

[11] J. Jin, *The Finite Element Method in Electromagnetics.* New York: Wiley, 1993.

[12] B. N. Parlett, *The Symmetric Eigenvalue Problems.* Englewood Cliffs, NJ: Prentice-Hall, 1980.

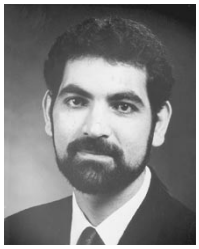

Mohammad R. Zunoubi (S'91–M'96) received the B.S. (honors) and M.S. degrees in electrical engineering from the University of Mississippi, University, MS, in 1989 and 1991, respectively, and the Ph.D. degree in electrical engineering from Mississippi State University in 1996.

From 1989 to 1992, he was a Research Assistant in the Department of Electrical Engineering, University of Mississippi. From 1992 to 1996 he was a Research Assistant and a Teaching Assistant in the Department of Electrical and Computer Engineering, Mississippi State University. Since September 1996 he has been a Postdoctoral Research Fellow at the Center for Computational Electromagnetics, University of Illinois, Urbana-Champaign. His research interest include the areas of computational electromagnetics, antennas, and electromagnetic compatibility.

Jian-Ming Jin (S'87–M'89–SM'94), for a photograph and biography, see p. 311 of the March 1998 issue of this TRANSACTIONS.

Kalyan C. Donepudi received the B.Tech degree in electrical engineering from the Nagarjuna University, Guntur, India, in 1995. He received the M.S. degree from the University of Illinois, Urbana-Champaign, in 1998. He is currently working toward the Ph.D. degree at the University of Illinois in electrical engineering.

His research interests are in general areas of computational electromagnetics.

Weng Cho Chew (S'79–M'80–SM'86–F'93), for a photograph and biography, see p. 245 of the February 1997 issue of this TRANSACTIONS.